

Electrochemical Properties of Hollow Spherical $\text{Na}_3\text{V}_2(\text{PO}_4)_3/\text{C}$ Cathode Materials for Sodium-ion Batteries

Chunmei Huang, Zonglin Zuo*, Jianqiu Deng*, Qingrong Yao, Zhongmin Wang,
Huaiying Zhou

School of Material Science and Engineering, Guilin University of Electronic Technology, Guilin,
541004, China

*E-mail: jqdeng@guet.edu.cn (Deng Jianqiu), zuozonglin@163.com (Zuo Zonglin)

Received: 17 May 2017 / Accepted: 28 July 2017 / Published: 12 September 2017

Hollow Spherical $\text{Na}_3\text{V}_2(\text{PO}_4)_3/\text{C}$ cathode materials were successfully synthesized by a simple spray drying method. The structure and morphology of the samples were characterized by X-ray diffraction (XRD), scanning electron microscopy (SEM) and transmission electron microscopy (TEM) analysis. The electrochemical properties of the samples were also tested in details by cyclic voltammetry, charge-discharge testing and AC impedance technique. The experimental results show that the $\text{Na}_3\text{V}_2(\text{PO}_4)_3$ can be indexed as rhombohedral structure and exhibits hollow spherical morphology. $\text{Na}_3\text{V}_2(\text{PO}_4)_3/\text{C}$ cathode materials deliver good rate performance and relative high discharge capacity. The discharge capacities are 96.8 and 70.9 mAh g^{-1} at the rate of 0.1C and 10C, respectively. And a stable capacity of 70 mAh g^{-1} is retained and the capacity retention is 75.7% after 200 cycles at 1C.

Keywords: $\text{Na}_3\text{V}_2(\text{PO}_4)_3/\text{C}$ composite; Sodium-ion batteries; Cathode; Hollow spherical structure

1. INTRODUCTION

There has been an urgent need to develop sustainable, green and low carbon energy such as solar radiation, wind and waves due to the escalating oil crisis and increasing environmental pollution. However, these renewable and cleaner energy sources are variable in time and diffuse in space, so it puts forward higher requirements for large energy storage technology [1-3]. Lithium-ion batteries (LIBs) are one of typical energy storage technologies, which have great potential in the field of electric vehicles (EV) and large-scale electric energy storage (EES) [3, 4]. In the past twenty years, lithium ion batteries have been successfully used in the portable devices and electric vehicles [5]. However, the problem of lithium resources deficiency and security matters which limits its large-scale application.

Compared with LIBs, sodium ion batteries (SIBs) have become a hot topic in the field of large-scale energy storage owing to their potential advantages, such as rich resources, high economy benefit and good safety [6].

Up to now, some electrode materials have been found to be applicable for sodium-ion battery (SIBs), such as NaMnO_2 [7], NaVPO_4F [8], $\text{Na}_{1.5}\text{VOPO}_4\text{F}_{0.5}$ [9], $\text{Na}_2\text{FePO}_4\text{F}$ [10], $\text{Na}_3\text{V}_2(\text{PO}_4)_3$ [11], and so on. Among various cathode materials, NASICON structured $\text{Na}_3\text{V}_2(\text{PO}_4)_3$ has a high theoretical capacity of 118 mAh g^{-1} and has been considered as an ideal cathode material for SIBs because of its stable structural, high cycle stability and working voltage [12]. However, the low intrinsic electronic conductivity of $\text{Na}_3\text{V}_2(\text{PO}_4)_3$ results in a low actual discharge capacity, poor rate capability and cycle performance, which restricts its practical application in SIBs [13].

In order to overcome the issue, various strategies have been employed to improve the electronic conductivity and electrochemical performance of $\text{Na}_3\text{V}_2(\text{PO}_4)_3$, such as carbon coating [14, 15], ion doping [16], nano-sized particles [9, 17], and porous structure [18]. Wang et al. [18] have successfully synthesized the honeycomb-structured hierarchical porous $\text{Na}_3\text{V}_2(\text{PO}_4)_3/\text{C}$ using a facile one-pot synthesis method. The composite has spherical particles with the diameter of $\sim 3 \mu\text{m}$ and delivers a high cycling stability with a capacity retention of 93.6% after 200 cycles. Even at 5C and 20C, the initial discharge capacities are 97.2 mAh g^{-1} and 80.2 mAh g^{-1} , corresponding to 86% and 71% of capacity at 0.2C, respectively. The porous structure benefits the electrolyte penetration and promotes ion transport pathways, thus leads to enhanced electrochemical performance of NVP/C.

In this paper, hollow spherical $\text{Na}_3\text{V}_2(\text{PO}_4)_3/\text{C}$ was synthesized via a simple spray-drying method. The experiment results confirmed that the hollow spherical structured $\text{Na}_3\text{V}_2(\text{PO}_4)_3/\text{C}$ exhibits good electrochemical performance. For comparison, porous $\text{Na}_3\text{V}_2(\text{PO}_4)_3/\text{C}$ was also synthesized by a hydrothermal method.

2. EXPERIMENTAL

2.1. Synthesis of Materials

In this study, hollow spherical $\text{Na}_3\text{V}_2(\text{PO}_4)_3/\text{C}$ (Sample A) was synthesized by spray-drying method. Firstly, 0.005 mol NH_4VO_3 and 0.0075 mol oxalic acid ($\text{C}_2\text{H}_2\text{O}_4 \cdot \text{H}_2\text{O}$) were dissolved in 200 mL of deionized water under vigorous stirring. Secondly, stoichiometric amount of Na_2CO_3 , $\text{NH}_4\text{H}_2\text{PO}_4$ and glucose were added to the mixed solution under vigorous stirring for 2 h to get a clear solution. The mixed solution was spray-dried to obtain the precursor powders. Finally, the products were obtained by heating at $350 \text{ }^\circ\text{C}$ for 4 h and sintering at $750 \text{ }^\circ\text{C}$ for 10 h in a tube furnace under reducing atmosphere ($\text{Ar}:\text{H}_2 = 95:5$).

The porous $\text{Na}_3\text{V}_2(\text{PO}_4)_3/\text{C}$ (Sample B) was synthesized by hydrothermal method. Firstly, 0.005 mol NH_4VO_3 and 0.0075 mol oxalic acid ($\text{C}_2\text{H}_2\text{O}_4 \cdot \text{H}_2\text{O}$) were dissolved in 80 mL deionized water under vigorous stirring. Secondly, stoichiometric amount of Na_2CO_3 , $\text{NH}_4\text{H}_2\text{PO}_4$ and glucose were added to the mixed solution under vigorous stirring at $60 \text{ }^\circ\text{C}$ for 2 h to get a clear solution. Finally, the mixed solution was transferred into Teflon-lined stainless steel autoclaves and maintained at 180

°C for 4 h. After the solution cooled to room temperature, then dried at 80 °C for 24 h and dried at 120 °C for 12 h in a vacuum oven to achieve the precursor powder. Then the same sintering process to sample A was used to prepare the Sample B.

2.2. Materials characterization

The crystal structure of samples was characterized by X-ray powder diffraction (XRD) technology using a D8 advance X-ray diffractometer with Cu K α radiation in the 2θ range of 10– 80° at a scan rate of 2° min⁻¹. The carbon content of the samples was determined by thermogravimetric (TG) analysis. The morphology of the samples was investigated by scanning electron microscope (FESEM, HitachiS-4800) and high-resolution transmission electron microscope (HRTEM, Tecnai G2 F20, 200 kV).

2.3. Electrochemical measurements

The electrochemical properties of Na₃V₂(PO₄)₃/C samples were conducted using a 2032-type coin cell. The working electrodes were prepared by mixing 80% of the active material, 20% of super carbon, and 10% PVDF (polyvinylidene fluoride) in N-methyl-2-pyrrolidone and casting on an aluminum foil, then drying at 110 °C for 12 h in vacuum condition. The electrolyte solution was 1 M NaClO₄ dissolved in ethylene carbonate (EC) and diethyl carbonate (DEC) (1:1 in volume). Sodium metal foil was used as the anode, a Celgard 2400 microporous membrane as the separator. Cells were assembled in an argon-filled glove box. The galvanostatic charge/discharge tests were performed with an Arbin battery testing system at different current densities between 3.0 and 4.3 V.

Cyclic voltammetry (CV) and electrochemical impedance spectroscopy (EIS) were carried on a Solartron electrochemical workstation.

3. RESULTS AND DISCUSSION

As shown in Fig. 1, the powder X-ray diffraction patterns of the samples could be indexed well as a single rhombohedral Na₃V₂(PO₄)₃ (PDF No. 01-070-3613) with a R $\bar{3}C$ space group. No other phases can be detected, confirming the high purity of the samples. Besides, no diffraction peaks related to the decomposed carbon, which indicates that the residual carbon is amorphous and has no effect on crystal structure of Na₃V₂(PO₄)₃.

SEM images of Na₃V₂(PO₄)₃/C are shown in Fig. 2a-b, respectively. It can be clearly seen that the sample A exhibits a hollow structure. The formation of hollow structure could be ascribed to product and release of large amount of H₂O, NH₃, and CO₂ during the sintering process, resulting in a hollow spherical morphology.

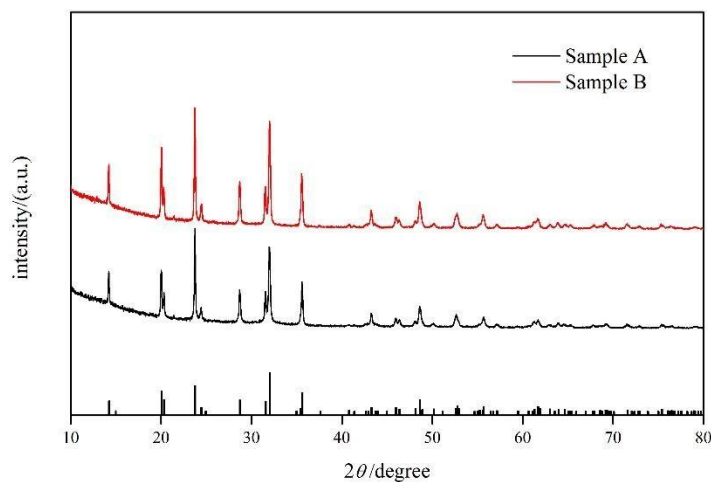


Figure 1. XRD patterns of samples

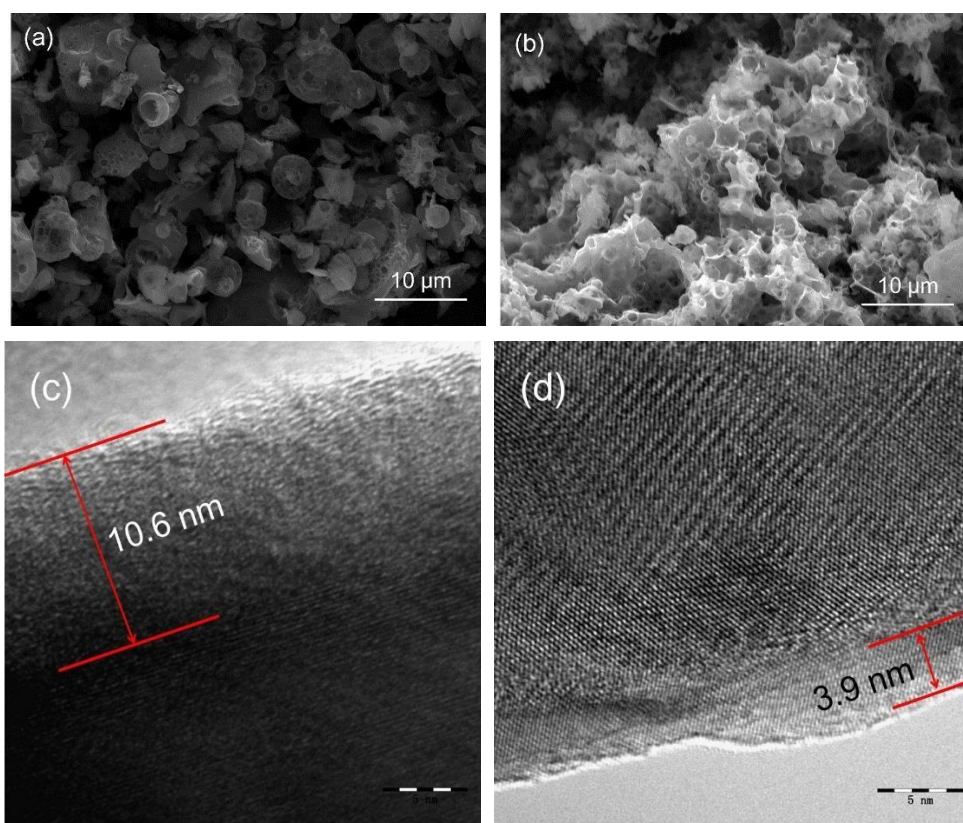


Figure 2. SEM and HRTEM images of samples A and B (a, c) Sample A; (b, d) Sample B

The residual carbon resulting from the precursor prevented the aggregation of particles. The morphology of sample B has a porous structure with a certain agglomerating. The hollow and porous structures are beneficial to the electrolyte penetration and the increase of sodium storage active sites, which effectively enhances electrochemical performance of $\text{Na}_3\text{V}_2(\text{PO}_4)_3/\text{C}$. The typical HRTEM images of sample A and B are shown in Fig. 2c-d, respectively. The TEM images demonstrate an

obvious core-shell structure and a carbon layer coating on the surface of $\text{Na}_3\text{V}_2(\text{PO}_4)_3$ particles, and the thickness of carbon layer is 10.6 nm and 3.9 nm, respectively. Compared to sample B, the sample A has a thicker and more uniform carbon layer. For the sample B, a partial glucose is transformed into carbon spheres the hydrothermal process and acting as reducing agent rather than carbon coating layer. The TG analysis also further verifies the higher carbon content in sample A. The thick carbon layer and high carbon content is beneficial to enhance the electronic conductivity of $\text{Na}_3\text{V}_2(\text{PO}_4)_3/\text{C}$, resulting in the improvement of the electrochemical performance.

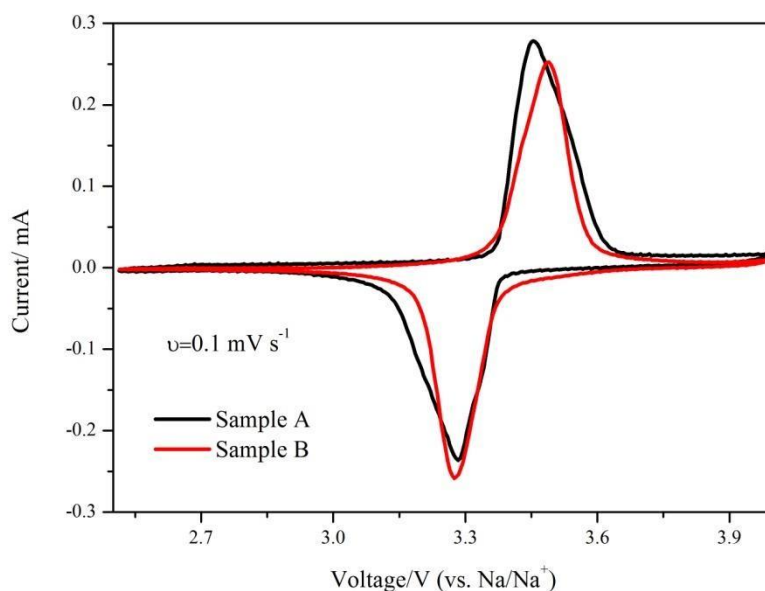


Figure 3. CV curves of the $\text{Na}_3\text{V}_2(\text{PO}_4)_3/\text{C}$ samples at a scan rate of 0.1 mV s^{-1} .

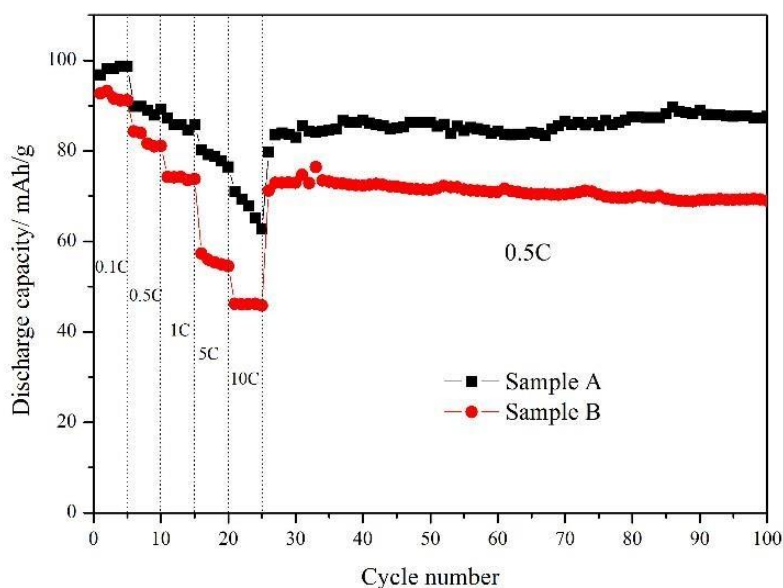


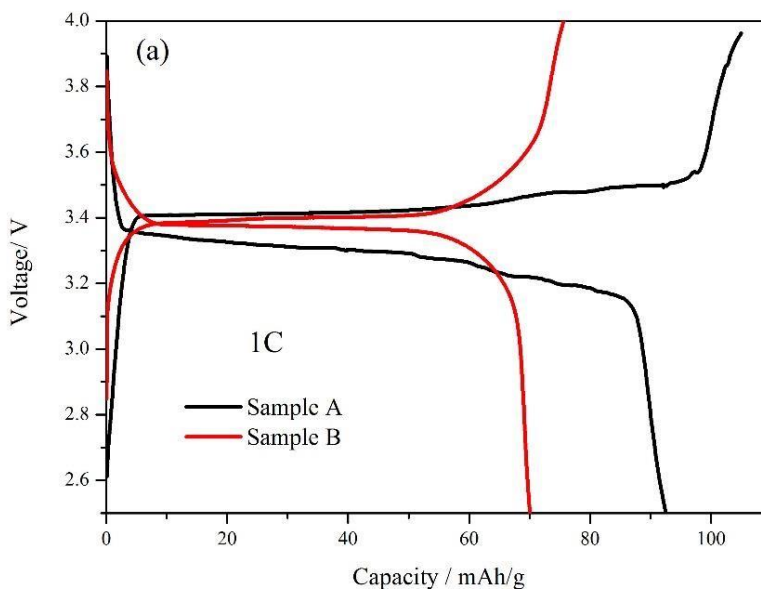
Figure 4. Rate capabilities of the $\text{Na}_3\text{V}_2(\text{PO}_4)_3/\text{C}$ samples in the range of 2.5–4.0 V.

Fig.3 shows CV curves of the $\text{Na}_3\text{V}_2(\text{PO}_4)_3/\text{C}$ samples at a scanning rate of 0.1 mV s^{-1} within the potential range of 2.5–4.0 V. Two samples show a pair of well-defined redox peak, indicating good

reversibility of sodium ion extraction/insertion in the samples. The potential of oxidization and reduction of the samples at around 3.4 V, which corresponds to the redox of V^{4+}/V^{3+} couple [9, 19]. The smaller redox peak potential difference in sample A can be observed, indicating the lower polarization and better rate capability.

The rate capability of the samples was evaluated by galvanostatic charge-discharge testing at different rates of 0.1C, 0.5C, 1C, 5C and 10C ($1C=118 \text{ mAh g}^{-1}$) in the voltage of 2.5–4.0 V. It can be clearly seen that the sample A exhibit a better rate and cycle performance. The discharge capacities are 96.8, 89.8, 87.2, 80.3 and 70.9 mAh g^{-1} at 0.1C, 0.5C, 1C, 5C and 10C, respectively. The capacity at high rates of 5C and 10C is higher than the previous result [20-23]. This better rate capability of the sample A may be due to the synergetic effect of hollow structure and high carbon content. The uniformly dispersed hollow spherical particles could increase the contact area between electrode and electrolyte and facilitate the charge transfer. The uniform carbon layer with high content can improve the electric conductivity of $\text{Na}_3\text{V}_2(\text{PO}_4)_3$, which is beneficial to improvement of rate capability. When the discharge current density is turned back to 0.5C, the discharge capacity can recover 79.8 mAh g^{-1} . The discharge capacity retaining 87.7 mAh g^{-1} after 100 cycles and the capacity retention of 97.6% (compare with the initial discharge capacity at 0.5C), indicating an excellent cycling stability of sample A.

Meanwhile, the long-term cycle stability of the hollow structural $\text{Na}_3\text{V}_2(\text{PO}_4)_3/\text{C}$ cathode under 1C was also explored. Fig. 5a shows the initial charge/discharge curves of two samples at 1C in the voltage range of 2.5–4.0 V. Two samples exhibit a well-defined charge/discharge plateau at approximately 3.4 V, corresponding to the reduction and oxidation peaks in the CV curves (see Figure 3). Compared to the sample B, the sample A delivers better long cycling stability with a high reversible capacity of 92.5 mAh g^{-1} and good capacity retention of 75.7% after 200 cycles at a rate of 1C, as shown in Fig. 5b. However, the capacities and cycling stability of sample A need to further improved compared with the previous results [9, 24-27]. This may be attributed to the sample A has certain level agglomerate phenomenon.



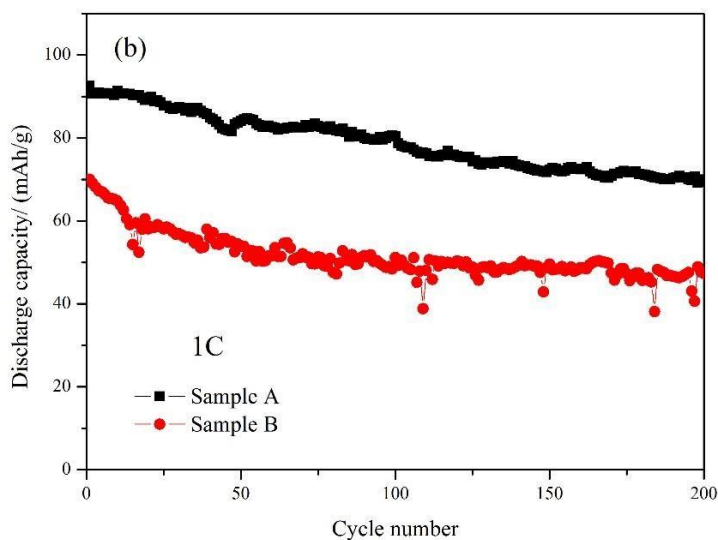


Figure 5. The charge/discharge curves and long-term cycling performance of $\text{Na}_3\text{V}_2(\text{PO}_4)_3/\text{C}$ samples. (a) Charge/discharge curves; (b) Cycling performance

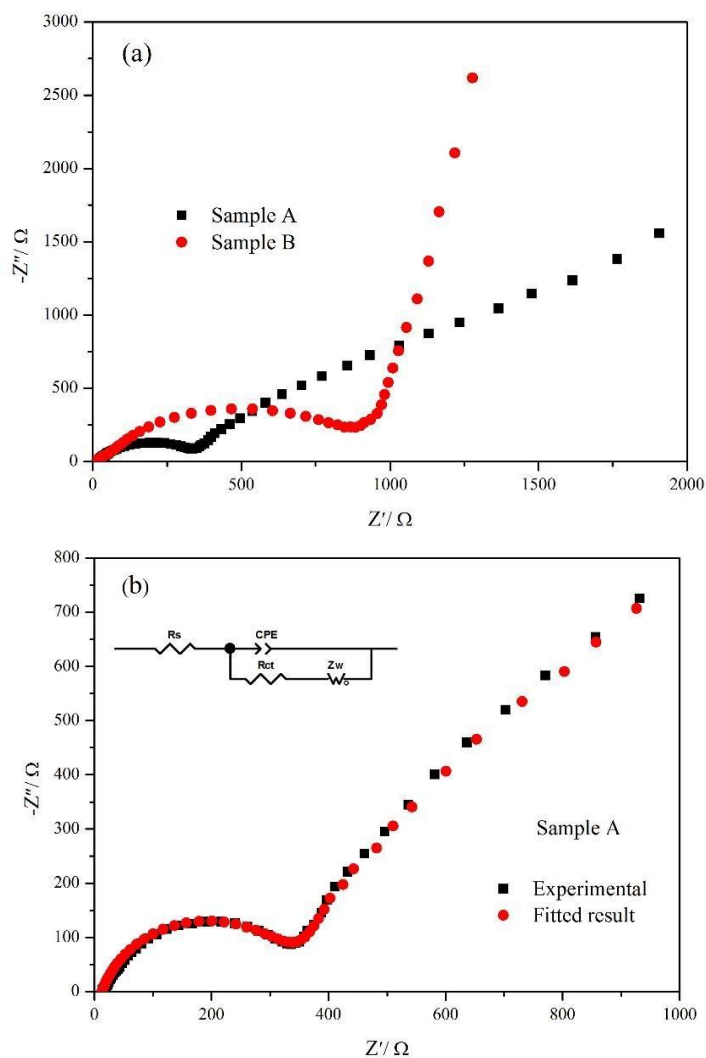


Figure 6. EIS spectra of $\text{Na}_3\text{V}_2(\text{PO}_4)_3/\text{C}$ samples. (a) EIS spectra; (b) Fitted result of EIS spectrum of sample A.

The relative low capacities and poor cycle stability in the sample B may be attributed to low carbon content and aggregate particles, resulting in that some active materials fail to participate in the reaction during charge-discharge process, as well as the conductivity of $\text{Na}_3\text{V}_2(\text{PO}_4)_3$ cannot be greatly enhanced. In addition, the nonuniform carbon layer cannot offer the well electrical contact between the active materials.

To clarify difference of electrochemical properties of two samples, AC impedance spectra of the cells at the fully discharge state after 200 cycles was measured by a Solartron electrochemical workstation in the frequency range from 10 mHz to 100 kHz with a potential perturbation at 5 mV. Fig. 6a shows the Nyquist plots of two samples. The electrochemical impedance spectra consist of the semicircle in the high frequency region, and a sloping line in the low frequency region. The AC impedance spectra is similar to the results of previous $\text{Na}_3\text{V}_2(\text{PO}_4)_3/\text{C}$ cathode materials [9, 19, 24]. The semicircle at high-frequency region is assigned to the charge transfer resistance (R_{ct}). The sloping line in the low frequency represents to the diffusion impedance of sodium ion in active materials. The impedance spectra were simulated by an equivalent circuit model as shown in Fig. 6b. The charge transfer resistance (R_{ct}) of two samples is 330 Ω and 890 Ω , respectively. The charge transfer resistance in sample A is lower than the previous reports [28], indicating a higher electrical conductivity and improving the rate capability and cycle stability.

4. CONCLUSIONS

In conclusion, the hollow spherical $\text{Na}_3\text{V}_2(\text{PO}_4)_3/\text{C}$ cathode material have been synthesized by a spray drying method. The hollow spherical $\text{Na}_3\text{V}_2(\text{PO}_4)_3/\text{C}$ sample exhibits good electrochemical performance with a reversible capacity of 96.8 mAh g^{-1} and a capacity retention of 75.7% after 200 cycles, which is ascribed to the hollow structure and uniform carbon layer. The spray drying method is suitable for large scale production of electrode materials, due to its merits with time-saving, simple process and easy operation.

ACKNOWLEDGEMENTS

This work was financially supported by the National Natural Science Foundation of China (No. 21363005, 51371061 and 51661009) and the Guangxi Natural Science Foundation (2016GXNSFGA380001). Chunmei Huang gratefully acknowledged the financial support from Guangxi Undergraduate Training Programs (201410595088). Zonglin Zuo thanked the financial support from Innovation Project of GUET Graduate Education (YJCXS201569).

References

1. C. Xu, B. H. Li, H. D. Du, F. Y. Kang, *Angew. Chem.* 51 (2012) 933.
2. G. L. Li, Z. Yang, Y. Jiang, W. X. Zhang, Y. H. Huang, *J. Power Sources* 308 (2016) 52.
3. W. F. Huang, S. Tao, J. Zhou, C. Si, X. Chen, W. Huang, C. H. Jin, W. S. Chu, L. Song, Z. Y. Wu, *J. Phys. Chem. C* 118 (2013) 796.
4. J. R. Ying, J. Gao, C. Y. Jiang, W. Li, C. P. Tang, *J. Inorg. Mater.* 21 (2006) 1097.

5. W. H. Li, Z. Z. Yang, Y. Jiang, Z. R. Yu, L. Gu, Y. Yu, *Carbon* 78 (2014) 455.
6. N. Yabuuchi, K. Kubota, M. Dahbi, S. Komaba, *Chem. Rev.* 114 (2014) 11636.
7. X. H. Ma, H. L. Chen, G. Ceder, *J. Electrochem Soc.* 158 (2011) 271.
8. Y. Lu, S. Zhang, Y. Li, L. G. Xue, G. J. Xu, X. W. Zhang, *J. Power Sources* 247 (2014) 770.
9. A. A. Tsirlin, R. Nath, A. M. Abakumov, Y. Furukawa, D. C. Johnston, M. Hemmida, H. -A. Krugvon Nidda, A. Loidl, C. Geibel, H. Rosner, *Phys. Rev. B: Condens. Matter.* 84 (2011) 44.
10. A. Langrock, Y. H. Xu, Y. H. Liu, S. Ehrman, A. Manivannan, C. S. Wang, *J. Power Sources* 223 (2013) 62.
11. Z. L. Chu, C. B. Yue, *Ceram. Int.* 42 (2015) 820.
12. S. Y. Lim, H. Kim, R. A. Shakoor, Y. S. Jung, J. W. Choi, *J. Electrochem. Soc.* 159 (2012) A1393.
13. Y. H. Jung, C. H. Lim, D. K. Kim, *J. Mater. Chem. A.* 1 (2013) 11350.
14. Y. Jiang, Z. Yang, W. Li, L. Zeng, F. Pan, M. Wang, X. Wei, G. Hu, L. Gu, Y. Yu, *Adv. Energy Mater.* 5 (2015)
15. L. Zhang, T. Huang, A. Yu, *J. Alloys Compds.* 646 (2015) 522.
16. H. Li, Y. Bai, F. Wu, Q. Ni, C. Wu, *Acs Appl. Mater. Inter.* 8 (2016) 27779.
17. H. Wang, D. Jiang, Y. Zhang, G. Li, X. Lan, H. Zhong, Z. Zhang, Y. Jiang, *Electrochim. Acta* 155 (2015) 23.
18. Q. Wang, B. Zhao, S. Zhang, X. Gao, C. Deng, *J. Mater. Chem. A.* 3 (2015) 7732.
19. Q. Zhang, W. Wang, Y. Wang, P. Feng, K. Wang, S. Cheng, K. Jiang, *Nano Energy* 20 (2014) 11.
20. J. Liu, K. Tang, K. P. Song, A. A. Peter, Y. Yu, J. Maier, *Nanoscale* 6 (2014) 5081.
21. J. Kang, S. Baek, V. Mathew, J. Gim, J. J. Song, H. Park, E. Chae, A. K. Rai, J. Kim, *J. Mater. Chem A* 22 (2012) 20857.
22. J. F. Mao, C. Luo, T. Gao, X. L. Fan, C. S. Wang, *J. Mater. Chem A* 3 (2015) 10378.
23. A. Chekannikov, R. Kapaev, S. Novikova, N. Tabachkova, T. Kulova, A. Skundin, A. Yaroslavtsev, *J Solid State Electr* 2017 1.
24. S. Tao, P. Cui, W. Huang, Z. Yu, X. Wang, S. Wei, D. Liu, L. Song, W. Chu, *Carbon* 96 (2016) 1028.
25. J. Q. Fang, S. Q. Wang, Z. T. Li, H. B. Chen, L. Xia, L. X. Ding, H. H. Wang, *J. Mater. Chem A* 4 (2016) 1180.
26. H. Li, C. Wu, Y. Bai, F. Wu, M. Z. Wang, *J. Power Sources* 326 (2016) 14.
27. Y. N. Xu, Q. L. Wei, C. Xu, Q. D. Li, Q. Y. An, P. F. Zhang, J. Z. Sheng, L. Zhou, L. Q. Mai, *Adv Energy Mater* 6 (2016) 1600389.
28. Q. Zhang, W. Wang, Y. J. Wang, P. Y. Feng, K. L. Wang, S. J. Cheng, K. Jiang, *Nano Energy* 20 (2016) 11.